HHS Public Access

Author manuscript

Biomacromolecules. Author manuscript; available in PMC 2023 December 12.

Published in final edited form as:

Biomacromolecules. 2022 December 12; 23(12): 5127–5136. doi:10.1021/acs.biomac.2c00873.

Metastatic Colon Cancer Treatment Using S100A9-Targeted Cowpea Mosaic Virus Nanoparticles

Young Hun Chung,

Department of Bioengineering and Moores Cancer Center, University of California, San Diego, La Jolla, California 92093-0021, United States

Britney A. Volckaert,

Department of NanoEngineering, University of California, San Diego, La Jolla, California 92093-0021, United States

Nicole F. Steinmetz*

Department of Bioengineering, Moores Cancer Center, Department of NanoEngineering, Department of Radiology, Institute for Materials Discovery and Design, Center for Nano-Immuno Engineering, and Center for Engineering in Cancer, University of California, San Diego, La Jolla, California 92093-0021, United States

Abstract

Peritoneal metastases (PMs) occur due to the metastasis of gynecological and gastrointestinal cancers such as ovarian, colon, pancreatic, or gastric tumors. PM outgrowth is often fatal, and patients with PMs have a median survival of 6 months. Cowpea mosaic virus (CPMV) has been shown, when injected intratumorally, to act as an immunomodulator reversing the immunosuppressive tumor microenvironment, therefore turning cold tumors hot and priming systemic antitumor immunity. However, not all tumors are injectable, and PMs especially will require targeted treatments to direct CPMV toward the disseminated tumor nodules. Toward this goal, we designed and tested a CPMV nanoparticle targeted to S100A9, a key immune mediator for many cancer types indicated in cancer growth, invasiveness, and metastasis. Here, we chose to use an intraperitoneal (IP) colon cancer model, and analysis of IP gavage fluid demonstrates that S100A9 is upregulated following IP challenge. S100A9-targeted CPMV particles displaying peptide ligands specific for S100A9 homed to IP-disseminated tumors, and treatment led to improved survival and decreased tumor burden. Targeting CPMV to S100A9 improves preclinical

*Corresponding Author: **Nicole F. Steinmetz** – *Department of Bioengineering, Moores Cancer Center, Department of NanoEngineering, Department of Radiology, Institute for Materials Discovery and Design, Center for Nano-Immuno Engineering, and Center for Engineering in Cancer, University of California, San Diego, La Jolla, California 92093-0021, United States;* nsteinmetz@ucsd.edu.

Supporting Information

The Supporting Information is available free of charge at https://pubs.acs.org/doi/10.1021/acs.biomac.2c00873.
S100A8/9 upregulation in ID8-*Defb29/Vegf-A*; characterization of dual fluorescent Cy5-CPMV-H6/G3 particles; photograph of dispersed nodules within the intraperitoneal space; Cy5-CPMV-H6/G3 tumor biodistribution repeat study; CPMV biodistribution in tumor homogenates; biodistribution of CPMV in all organs; clearance of CPMV within the intraperitoneal space; additional confocal images of tumor sections; and colocalization and Mander's coefficient of CPMV with S100A9 (PDF)

Complete contact information is available at: https://pubs.acs.org/10.1021/acs.biomac.2c00873

The authors declare the following competing financial interest(s): Dr. Steinmetz is a cofounder of, has equity in, and has a financial interest with Mosaic ImmunoEnginering Inc. Dr. Steinmetz serves as Director, Board Member, and Acting Chief Scientific Officer, and paid consultant to Mosaic. The other authors declare no potential COI.

outcomes and harbors the potential of utilizing CPMV for the treatment of IP-disseminated diseases.

Graphical Abstract

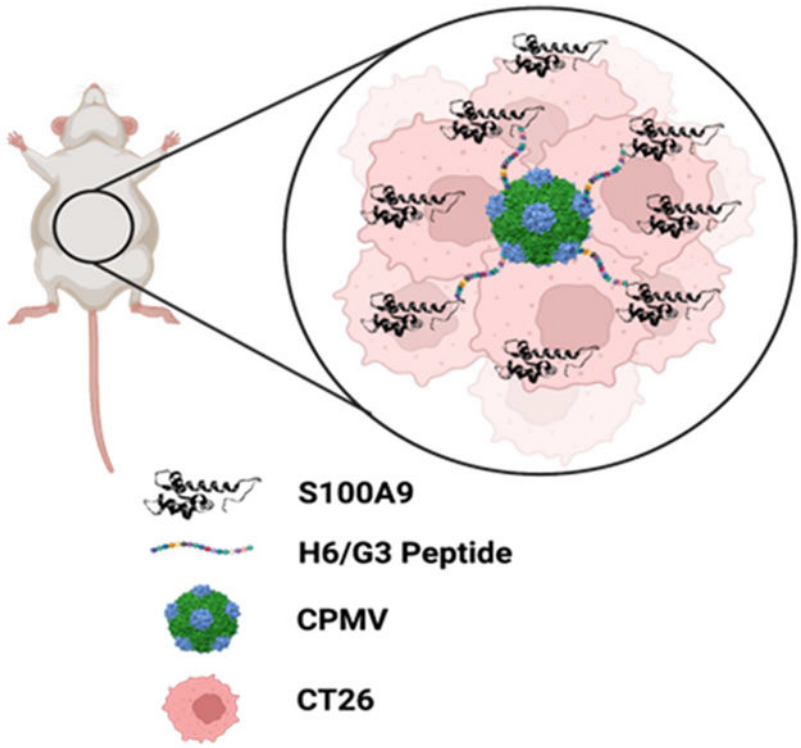

INTRODUCTION

Peritoneal metastases (PMs) are the result of metastasized tumors of gynecological or gastrointestinal origin.[1] PMs are difficult to diagnose due to their small volumes and inability of common imaging techniques such as MRI or CT to find the PMs.[2] Once PMs occur, they carry poor prognoses and are oftentimes fatal with a median survival of only 6 months in patients.[1] PMs are extremely common and can occur due to a wide range of cancers including colon, ovarian, gastric, pancreatic, and appendiceal tumors. In gastric cancer, PMs occur in up to 60% of patients,[3] while in colon and ovarian, the rates of PM occurrence are 40–80 and 50–75%, respectively.[4–6] In pancreatic cancer, the PM rates are around 50%, and pancreatic cancer patients with PMs only have an overall survival of 7–8 months.[7,8] The efficacy of systemically administered chemotherapeutics in treating PMs is extremely low and in fact, in colon cancer, patients with PMs are oftentimes excluded from clinical trials.[9] Such exclusion leads to an inherent bias in approved therapies toward “easier-to-treat” cancers, which is not representative of the population of patients.[9] Therefore, to improve quality of life and overall survival in patients with PMs, it is imperative that new technologies that can treat PMs and are developed for the specific treatment of PMs are continuously investigated.

Currently, the gold standard for treatment of PMs is either systemically or intraperitoneally (IP) administered chemotherapeutics. Systemically administered chemotherapeutics suffer from low bioavailability, treatment resistance, and dose-limiting toxicity.[10,11] Treatment leads to initial remission, but relapse of the tumors occurs in >70% of patients with advanced disease.[12] Relapsed tumors are treated primarily with additional chemotherapeutics, but at this stage, ascites formation can cause chemoresistance and overall treatment ineffectiveness.[13] While IP-administered chemotherapeutics have offered some benefit in improving survival, they still suffer from similar pitfalls such as local toxicities and continued low rates of overall survival. Furthermore, morbidity outcomes in a randomized trial show that direct intraperitoneal administration led to more side effects.[14]

Immunotherapeutic options have not been extensively explored in the treatment of PMs and such alternatives may be better suited, as they can lead to systemic rejection of cancer and prevention of metastatic outgrowths in other organs.[15] For instance, the cowpea mosaic virus (CPMV) has been explored as an immunomodulator for cancer therapy via in situ vaccination. CPMV is a plant picornavirus; it measures 28 nm in diameter and is composed of 60 copies each of a small and large coat protein of 24 and 42 kDa, respectively.[16] While noninfectious in mammals, its repetitive, proteinaceous capsid acts as a pathogen-associated molecular pattern (PAMP) that is recognized by immune cell pathogen recognition receptors (PRRs). Specifically, we have shown that the CPMV capsid triggers the toll-like receptors (TLRs) 2 and 4 and that the single-stranded RNA within CPMV activates TLR 7.[17] Receptor signaling cascades lead to the release of immunostimulatory cytokines such as interleukin (IL)-1β, IL-12, interferon (IFN)-γ, chemokine ligand 3, macrophage inflammatory protein-2, and granulocyte-macrophage colony-stimulating factor.[18,19] Specifically in a PM ovarian cancer model, IP-administered CPMV has been shown to increase the number of tumor-infiltrating neutrophils, dendritic cells, natural killer cells, and M1 macrophages within the intraperitoneal space.[20] Tumor cells are killed by these activated innate immune cells, which then also process the released tumor associated antigens and neoantigens. This leads to priming of CD4+ and CD8+ T cell responses and establishment of immune memory. Our previous research has shown that when injected intratumorally, CPMV-mediated immunostimulation can hinder tumor progression and lead to tumor cell death of multiple murine cancer types including melanoma, breast, colon, glioma, and ovarian[18,21–23] as well as spontaneous melanoma and inflammatory mammary cancer in canine patients.[24,25]

However, the aforementioned studies were limited to injectable tumors, and recently, we have expanded the capabilities of CPMV by modifying the CPMV capsid with peptides (called H6 and G3) that bind to a molecule called S100A9 for systemically administered targeted treatments.[26,27] These H6 and G3 peptides were found in previous work through phage display to bind to S100A9. The authors utilized the peptides for directing therapeutic peptibodies. Specifically, H6 and G3 peptides were fused to IgG2b antibodies to deplete S100A9-expressing myeloid-derived suppressor cell populations within the blood and tumor leading to delayed tumor growth in an EL4 lymphoma model.[27] Similarly, past research done in our lab has utilized the H6 and G3 peptide to target S100A9 in both cancer and cardiovascular applications. Intravenous injection of CPMV-H6 and CPMV-G3 led to homing to the lung microenvironment, which natively expresses S100A9, leading to

both prevention and treatment of lung metastasis from breast cancer and melanoma.[26] Importantly, the immunotherapeutic effects were unique to CPMV. Conjugating the peptides to a nonimmunogenic virus called the cowpea chlorotic mottle virus, which has the same size, shape, and charge, and is grown in the same plants as CPMV demonstrated no efficacy in reducing tumor burden. The peptides themselves also impart no immunotherapeutic efficacy and act solely as targeting modalities as demonstrated by past in vitro immunogenic assays.[26] We have also explored S100A9 targeting in cardiovascular disease using other S100A9-targeting peptides and the viruses CPMV and the tobacco mosaic virus, which led to increased viral load within the S100A9-rich deep vein thrombi and reduced thrombotic mass.[28]

S100A9 was chosen as the target molecule due to its overexpression in a variety of cancers.[29] S100A9, otherwise known as myeloid-related protein 14, is a calcium-binding damage-associated molecular pattern molecule that works as an immunomodulator in many immune disorders.[30] It is oftentimes found in a heterodimer form with its partner molecule S100A8 but can also form homodimers and heterotetramers (again with S100A8).[31,32] S100A9 overexpression has been demonstrated in breast, ovarian, skin, bladder, pancreatic, gastric, esophageal, colon, glioma, cervical, hepatocellular, and thyroid cancers.[33] It is expressed in neutrophils, monocytes, macrophages, and within the tumor stroma and can make up 40–50% of the cytosolic content within these cells.[29,33] It can be expressed, secreted, or displayed within the tumor microenvironment (TME), usually at extremely high concentrations, making it a prime target within the TME.[34,35] When the S100A8/9 axis becomes dysregulated as is the case for cancer, it potentiates protumor pathways increasing tumorigenesis, tumor aggressiveness, metastasis, and resistance to chemotherapeutics.[36–39] Lastly, S100A9 can play a prognostic role, and patients with high serum S100A9 expression or high levels of S100A9+ cells usually have lower survival rates and higher risks of recurrence.[40,41]

The current work explores the utility of the S100A9-targeted CPMV formulations in the treatment of PMs, specifically those of colon origin. While already demonstrating efficacy in metastatic melanoma and breast cancer, expanding the useability of the targeted CPMV solutions toward other metastatic cancers will allow us to utilize CPMV for a broader range of applications in the future. We evaluate S100A9-targeted CPMV treatment efficacy in a mouse model of metastatic colon cancer (CT26 in BALB/C) and demonstrate the ability of such targeted treatments to home to and localize in colon cancer tumor nodules inducing immunostimulation and ultimately leading to reduction of tumor burden.

MATERIALS AND METHODS

Materials and Cells.

Potassium phosphate monobasic and dibasic salts, 20× 3-morpholinepropane-1-sulfonic acid (MOPS) buffer, methanol, bovine serum albumin (BSA), and acetic acid were purchased from Fisher Scientific. Dimethyl sulfoxide (DMSO) and sucrose were purchased from Sigma-Aldrich, 10× phosphate buffered saline (PBS) was purchased from G-Biosciences, and sulfo-cyanine5-*N*-hydroxysuccinimide ester (sulfo-Cy5-NHS) was purchased from Lumiprobe.

CT26 cells were maintained in RPMI-1640 supplemented with 10% (v/v) fetal bovine serum (FBS) and 1% (v/v) penicillin/streptomycin. The CT26 cells were also engineered to express luciferin to enable luminescence imaging on the IVIS. ID8-*Defb29/Vegf-A* cells were maintained in RPMI-1640 supplemented with 10% (v/v) FBS, 2 mM L-glutamine, 1 mM sodium pyruvate, 0.05 mM 2-mercaptoethanol, and 1% (v/v) penicillin/streptomycin. FBS and penicillin/streptomycin were purchased from Cytiva. Sodium pyruvate was purchased from Thermo Fisher, and 2-mercaptoethanol was purchased from Sigma-Aldrich. The cells were maintained at 37 °C at 5% CO_2 levels.

Production of S100A9-Targeted CPMV Nanoparticles.

CPMV was isolated from infected black eyed pea plants as done previously.[49] CPMV was stored in 100 mM potassium phosphate (KP) buffer pH 7.2 at 4 °C until later use. The H6 (MEWSLEKGYTIKGGGSC) and G3 (WGWSLSHGYQVKGGGSC) peptides were purchased from Gen-Script Biotech (San Diego), stored in DMSO, and conjugated to the CPMV nanoparticles (VNPs) as previously reported.[26] In brief, an $SMPEG_8$ linker diluted in DMSO was added to CPMV at 5 equivalents per coat protein (CP) and incubated at room temperature (RT) for 2 h. The excess linker was removed through ultracentrifugation at 52,000 *g* for 1 h with a 40% (w/v) sucrose cushion. The pellet was resuspended in 10 mM KP (pH 7.2), and 1 equivalent per CP of the H6 or G3 peptide was added and reacted for 2 h at RT. The excess peptide was removed using a Sephadex G-25 MidiTrap column (Cytiva), and the resulting CPMV-H6 and CPMV-G3 were stored at 4 °C until further use.

Characterization of S100A9-Targeted CPMV Nanoparticles.

Ultraviolet–Visible (UV–vis) Spectroscopy.—The concentrations of CPMV, CPMV-H6, and CPMV-G3 were determined using UV–vis (NanoDrop). The absorbance values at 260 and 280 nm were measured, and the concentration of CPMV within the sample was calculated using the 260 nm wavelength and Beer's Law with an extinction coefficient of 8.1 mL mg^{-1} cm^{-1}. The ratio of 260–280 nm (260, 280^{-1} of ~1.8) was used to determine the absence of broken particles and protein contaminants within the samples.

Sodium Dodecyl Sulfate-Polyacrylamide Gel Electrophoresis (SDS-PAGE).—Both of the S100A9-targeted CPMV nanoparticles and wild type native CPMV were diluted in 10 mM KP and loaded with 4× lithium dodecyl sulfate sample buffer (Life Technologies) for a total concentration of 10 μg in 16 μL. CPMV was incubated at 95 °C for 5 min before loading onto a 12% NuPAGE gel (Thermo Fisher Scientific). The gels were run at 200 V, 120 mA, and 25 W for 40 min in 1× MOPS buffer, and the protein stains were visualized using GelCode Blue Stain reagent (Thermo Fisher Scientific) according to manufacturer's instructions. The gels were then imaged under an AlphaImager System (ProteinSimple).

Agarose Gel Electrophoresis.—The native and S100A9-targeted CPMV samples were diluted to a final concentration of 10 μg in 30 μL and run through a 1.2% (w/v) agarose gel stained with GelRed nucleic acid gel stain (Gold Biotechnology). The parameters were set at 120 V and 400 mA for 30 min. The RNA within the CPMV was imaged using the AlphaImager System, and the gel was then stained overnight in 0.25% (w/v) Coomassie Blue followed by destaining in a solution of deionized water, methanol, and acetic acid in

a 50:40:10 (v:v:v) ratio. The resulting protein bands were imaged using the AlphaImager System.

Dynamic Light Scattering (DLS).—The size of the nanoparticles was measured using a Zetasizer Nano ZSP/Zen5600 (Malvern Panalytical) system. The samples were diluted to 0.1 mg mL^{-1} in 10 mM KP and run at RT.

Fast Protein Liquid Chromatography (FPLC).—FPLC (ÄKTA pure 25 M1, Cytiva) was used to determine the structural integrity and purity of the CPMV, CPMV-H6, and CPMV-G3 samples. The samples were diluted to a final concentration of 0.3 mg mL^{-1} in 500 μL of 10 mM KP and run through a Superose 6 size exclusion column with dimensions of 10 × 300 mm. The flow rate was set to 0.5 mg mL^{-1} with an isocratic elution profile for a total elution volume of 50 mL, and absorbance measurements were taken at 260 and 280 nm to measure the nucleic acid and protein concentrations, respectively. The ratio of the absorbance values at 260 and 280 nm at the elution peak was calculated and compared to the UV–vis values to ensure the structural integrity of the VNPs.

ELISA of S100A8/9 Upregulation Following Colon Cancer Challenge.

All mice experiments were carried out according to the guidelines set out by the Institutional Animal Care and Use Committee at the University of California, San Diego, according to protocol number S18021. The animals were purchased from Jackson Laboratory and stored at the Moores Cancer Center and provided with unlimited food and drink.

To ensure the presence and expression of S100A9 within the intraperitoneal space of mice following colon cancer injection, enzyme linked immunosorbent assays (ELISAs) were carried out on intraperitoneal gavages of BALB/C mice. Female BALB/C mice ($n = 9$) at 6–7 weeks old were purchased, and three of the nine mice were immediately euthanized for intraperitoneal gavage. The rest of the mice were injected IP with 500,000 CT26 cells in 200 μL of PBS. Successful implantation of CT26 tumors was verified by injecting 150 mg kg^{-1} of D-luciferin (Gold Biotechnology) IP and imaged using the in vivo imaging system (IVIS) by Xenogen. The intraperitoneal fluid from the naïve mice was spun down at 10,000 *g*, and the supernatant was collected and stored at −80 °C until further use. Two weeks after tumor injection, three more mice were euthanized and the intraperitoneal fluid was collected and stored as before. This was then repeated once more at the week 3 time point. The intraperitoneal fluid was then analyzed using a mouse S100A8/9 DuoSet ELISA detection kit (R&D Systems) according to manufacturer's instructions. An S100A8/9 kit was utilized as opposed to a monomeric S100A9 kit as S100A9 is mainly found within the body in its heterodimer form with S100A8.[30]

ELISA analysis of intraperitoneal gavage was further carried out in ID8-*Defb29/Vegf-A* inoculated mice. Female C57BL/6 J mice that were 6–7 weeks old were injected IP with 2×10^6 cells in 200 μL of PBS, and the intraperitoneal fluid was collected at weeks 4, 6, and 8. The intraperitoneal fluid was also collected in naïve mice. The intraperitoneal fluid was then analyzed by ELISA for S100A8/9 identically as before.

Colon Cancer Treatment Using S100A9-Targeted CPMV.

The efficacy of S100A9-targeted CPMV was compared to native CPMV and controls in an intraperitoneal model of CT26. BALB/C mice at 6–7 weeks old were injected IP with 500,000 CT26 cells in 200 μL of PBS. One week following tumor injection, mice were separated into native CPMV, CPMV-H6, CPMV-G3, PBS, H6 peptide only, and G3 peptide only groups ($n = 5$ per group) and injected with 200 μg of VNP diluted in 200 μL of PBS. The amount of H6 or G3 peptides injected was determined through densitometry analysis of the SDS-PAGE gels (ImageJ). The mice were reinjected at weeks 2 and 3 for a total of three injections. The circumference and body weight of the mice were measured every two days starting from the eighth day following tumor cell injection, and the survival of the mice was also followed. Mice were euthanized when their body weight fold change exceeded 75% of their original body weight or 30 g (whichever came first) or their circumference fold change exceeded 60% of their original circumference.

Biodistribution of CPMV Particles Following Intraperitoneal Injection.

To follow the biodistribution of CPMV within the reticuloendothelial organs and tumors, dual fluorescent and S100A9-targeted CPMV particles were produced. In these particles, equal molar excesses (5 equivalents per CP) of sulfo-Cy5-NHS (Cy5) and $SMPEG_8$ were added concomitantly, and excess Cy5 and $SMPEG_8$ were removed using ultracentrifugation as before. The H6 and G3 peptides were added to only the peptide-conjugated CPMV samples, and the excess peptide was purified. For fluorescent CPMV without S100A9 targeting, 5 equivalents per CP of sulfo-Cy5-NHS was added without $SMPEG_8$. The particles were then analyzed using the same characterization methods as before except fluorescent imaging was also undertaken during the agarose and SDS-PAGE characterization steps. For the UV–vis and FPLC, absorbance measurements were also taken at 647 nm, and the amount of conjugated Cy5 per CPMV was calculated from UV–vis using Beer's Law and the molar extinction coefficient of Cy5 (270,000 cm^{-1} M^{-1}).

Female BALB/C mice were then injected IP with 500,000 CT26 cells in 200 μL of PBS. After 1 week, 200 μg of the Cy5-CPMV, Cy5-CPMV-H6, and Cy5-CPMV-G3 particles diluted in 200 μL of PBS and a PBS control were injected IP ($n = 5$), and dispersed tumor nodules were harvested from throughout the intraperitoneal space the following day. The tumors were imaged using the IVIS, and fluorescence counts within the tumors were calculated using region of interest (ROI) measurements within Living Image 3.0 software. In a separate study, the lungs, liver, kidneys, spleen, and tumors were harvested ($n = 3$) following injection of particles and PBS ($n = 3$) and imaged and quantified on the IVIS as before. This experiment was also repeated in naïve mice without tumor burden to compare biodistribution across the organs in both tumor-bearing and naïve mice. Following imaging, the tumors were weighed and then homogenized with a hand-held homogenizer (PerkinElmer) in 1 mL of PBS. The samples were spun down at 10,000 *g* for 10 min, and the supernatant was collected and read using a Tecan plate reader at 647 nm absorbance.

Confocal Imaging of Tumor Nodules Following CT26 Injection.

Female BALB/C mice were injected IP with 500,000 CT26 cells in 200 μL of PBS followed by injection with 200 μg of Cy5-CPMV, Cy5-CPMV-H6, and Cy5-CPMV-G3 IP. Tumor

nodules were then harvested after 24 h and snap frozen in liquid nitrogen and stored at −80 °C until further use. The tumors were moved into Tissue-Tek optimal cutting temperature (OCT) medium (Sakura) and sectioned into 10 μm sections on a Leica CM1860 cryostat. The remaining OCT medium was removed by submerging the slides in PBS for 3 min, and the slides were fixed in ice-cold methanol for 10 min at RT. The methanol was removed and washed with PBS three times with 5 min incubations. The slides were then blocked with 10% (w/v) BSA diluted in PBS for 1 h at RT followed by three washes with PBS.

A primary antibody solution of an α-S100A9 rabbit antibody (R&D Systems) was prepared by diluting 1:100 in a 1% (w/v) BSA solution in PBS and incubating the solution overnight at 4 °C. The slides were washed the next day, and a secondary antibody solution composed of a 1:200 dilution of α-rabbit goat AlexaFluor 555 antibody (Invitrogen) in PBS was incubated for 1 h at RT. The slides were washed and incubated with 5 μg mL^{-1} of Hoechst 3342 in PBS for 10 min. Hoechst 3342 was washed away, and the slides were allowed to dry in a dark chamber. After fully drying, the slides were mounted onto coverslips with 20 μL of Fluoroshield and imaged on a Nikon A1R Confocal/TIRF STORM microscope.

Statistical Analysis.

All the data were analyzed without preprocessing. Sample size (n) of the ELISA, biodistribution, and colocalization experiments were all $n = 3$, while the CT26 treatment experiments were all done at $n = 5$. Column graphs were analyzed using one-way ANOVA, while scatter plots were analyzed using two-way ANOVA with Tukey's multiple comparison test. The survival curve was analyzed using a log-rank (Mantel-Cox) test. All analyses were done on GraphPad Prism, and significance was deemed as any p value <0.05.

RESULTS AND DISCUSSION

Production and Characterization of CPMV-H6/G3 Nanoparticles.

CPMV-H6 and CPMV-G3 nanoparticles were generated as described previously.[26] In short, an $SMPEG_8$ linker was conjugated to the exterior lysines of CPMV nanoparticles followed by conjugation of the S100A9-targeting H6 (MEWSLEKGYTIKGGGSC) and G3 (WGWSLSHGYQVKGGGSC) peptides (Figure 1a). An intervening GGGSC linker was added to the H6 and G3 peptides to allow for maleimide conjugation and greater peptide chain flexibility. Characterization of the CPMV-H6/G3 nanoparticles was first carried out with ultraviolet–visible spectroscopy (UV–vis), and the absorbance at 260 and 280 nm corresponding to the RNA and protein within the samples, respectively, was measured (Figure 1b). The absorbance ratio of 260–280 is a direct indicator of the purity of the nanoparticles; for CPMV, a 260:280 ratio of 1.8 demonstrates a pure solution. Indeed, all of our samples (CPMV, CPMV-H6, and CPMV-G3) had 260–280 absorbance ratios close to the ideal value of 1.8 (Figure 1b). The samples were further analyzed by SDS-PAGE (Figure 1c). CPMV is composed of 60 copies each of a small (S) and large (L) CP of 24 and 42 kDa, respectively, in a pseudo $T = 3$ symmetry.[16] For CPMV-H6/G3 additional higher molecular weights, bands above the S and L protein are detectable which correspond to conjugated, peptide-displaying CPs. Using the ImageJ band analysis tool, 20.0 and 20.5% of the CPs were conjugated for CPMV-H6/G3, respectively corresponding to 24 and 25

peptides per particle. Agarose gel electrophoresis (Figure 1d) was also carried out, which showed identical electrophoretic mobility of both the RNA (left) and protein (right) bands indicating stable, unbroken particles. There were also no aggregates as seen by the lack of smearing or higher mobility bands. DLS (Figure 1e) and FPLC (Figure 1f) reiterate the presence of stable, uniform particles—there was no indication of broken particles or aggregation. The size of the S100A9-targeted CPMV was slightly greater than that measured for CPMV with 32.94 and 34.53 nm for CPMV-H6 and CPMV-G3, respectively, vs 31.08 nm for CPMV, but the low polydispersity indices (PDIs) validate particle monodispersity.

S100A8/9 Levels in the Intraperitoneal Space.

S100A8/9 levels within the intraperitoneal space following CT26 tumor challenge was measured through ELISA analysis. The heterodimer form of S100A8/9 was analyzed in contrast to homomeric S100A9 as S100A9 is most commonly found within the body in its heterodimer form.[30] The intraperitoneal fluid was collected prior to tumor injection in naïve mice through intraperitoneal gavage as well as 2 and 3 weeks following intraperitoneal injection of 500,000 CT26 cells (Figure 2a). The intraperitoneal fluid was centrifuged to remove cellular debris, and the supernatant was collected and analyzed. ELISA results indicate that in naïve mice, S100A8/9 is not detected within the intraperitoneal space; however, following tumor injection, S100A8/9 production begins to dramatically increase with average S100A8/9 concentrations reaching 129.4 and 256.8 pg mL^{-1} by weeks 2 and 3, respectively (Figure 2b). The complete ELISA analysis is shown in Figure 2c. To further assess the potential for S100A9-targeted delivery of CPMV nanoparticles in other metastatic cancer models, we also demonstrated S100A8/9 upregulation within the intraperitoneal fluid up to 8 weeks following metastatic ovarian cancer injection (Figure S1).

Previous reports have shown that S100A8/9 is upregulated in colon cancer, and our data help validate these findings.[42,43] It was shown that S100A8/9 was absent in healthy colon tissue, and similarly, we saw no evidence of S100A8/9 within the intraperitoneal space of naïve mice (Figure 2b).[44] S100A8/9-positive myeloid progenitor cells can directly release S100A8/9 into the TME and interact with receptors for advanced glycation end-product (RAGE) and carboxylated N-glycans on CT26 colon cancer cells and myeloid-derived suppressor cells (MDSCs).[44,45] These interactions most likely promote S100A8/9 retention and upregulation within the intraperitoneal space, and our data as well as the previous literature point to the potential for S100A9-targeted delivery of our CPMV nanoparticles. Although we focus on colon cancer, we also envision that the therapy has potential for the treatment of other IP-disseminated cancers. We and others have shown that S100A9 becomes upregulated in ovarian (Figure S1) and gastric cancer, which are known to form PMs.[1,33]

Treatment of Metastatic CT26 Cancer with S100A9-Targeted CPMV.

Due to the upregulation of S100A8/9 by CT26, we hypothesized that S100A9-targeted CPMV would home to IP-disseminated colon cancer tumor nodules and induce potent efficacy compared to native CPMV. To test this, we injected 500,000 CT26 cells IP followed by weekly intraperitoneal injections of 200 μg of CPMV, CPMV-H6, CPMV-G3, H6, G3 (free peptide concentration was normalized to the amount of the conjugated peptide,

see Figure 1c), and PBS for a total of three injections (Figure 3a). The body weight, circumference, and survival of the mice were analyzed every 2 days. Colon cancer growth within the intraperitoneal space leads to ascites formation, which causes buildup of blood and other fluids within the intraperitoneal space leading to enlarged circumferences and increased body weight.[46] The data show that the negative controls of PBS, H6, and G3 were unable to prevent or slow down the growth of the tumors, and all the mice within those groups had to be sacrificed by day 25 due to reaching clinical endpoints (Figure 3b). The body weight (Figure 3c) and the circumference (Figure 3d) of the mice grew unabated while the body weight and circumference of the S100A9-targeted CPMV treatment groups remained fairly stable. By day 17, the average circumference of the PBS, H6, G3, and native CPMV had reached 6.60, 6.78, 7.03, and 6.32 cm, respectively. On the contrary, the average circumference of the CPMV-H6 and CPMV-G3 mice measured at 5.50 and 5.16 cm, respectively. The starting average circumference of the CPMV-H6 and CPMV-G3 mice were 5.18 and 5.22 cm meaning that even after CT26 injection, the average circumference had only risen by 6.2% in the CPMV-H6 group and had remained stable within the CPMV-G3 group. Compared to PBS and H6, the CPMV-H6 treatment decreased the average circumference by 20 ($p < 0.0001$) and 23.3% ($p < 0.0001$), respectively. CPMV-G3 decreased the average circumference compared to PBS and G3 by 26.4 ($p < 0.0001$) and 34.7% ($p < 0.0001$).

Using the treatment schedule and dose, native CPMV had moderate levels of efficacy as evident by the reduced body weight and circumference vs the PBS control with one mouse surviving up to 37 days. However, S100A9-targeted CPMV-H6/G3 clearly outperformed native CPMV. For instance, at day 27, the average circumference in CPMV groups was 7.1 cm while CPMV-H6 and CPMV-G3 were 5.7 and 5.1 cm corresponding to a 24.6 ($p < 0.001$) and 39.2% ($p < 0.0001$) discrepancy, respectively. Enhanced efficacy of CPMV-H6 and CPMV-G3 vs CPMV was also reflected by increased survival: the median survival for the CPMV-H6, CPMV-G3, CPMV, PBS, H6, and G3 were 43, 54, 29, 21, 25, and 23 days post tumor inoculation, respectively. When relating CPMV-H6 to PBS, H6, and CPMV, the median survival increased by 2.1-fold ($p < 0.01$), 1.7-fold ($p < 0.01$), and 1.5-fold ($p = 0.059$), respectively. CPMV-G3 showed similar survival benefit increasing the median survival by 2.6-fold ($p < 0.05$), 2.3-fold ($p < 0.05$), and 1.9-fold ($p < 0.05$) compared to PBS, G3, and CPMV, respectively.

It is important to note that the H6 and G3 peptides do not increase the immunogenicity of the CPMV nanoparticles and that they only aid in localizing the CPMV to areas of tumor progression.[26] In a RAW-Blue assay, the H6 and G3 peptides were unable to elicit any immunogenic response.[26] While native CPMV can delay tumor growth, it is the targeting that imparts the added efficacy. Past ovarian cancer studies using native CPMV have demonstrated that CPMV induces the upregulation of immunostimulatory cytokines such as IFNγ and IL-6 while decreasing levels of immunosuppressive cytokines like IL-10 and TGFβ.[20] This improves the accumulation of antitumor immune cells such as natural killer cells, M1 macrophages, neutrophils, and dendritic cells leading to tumor death. By targeting CPMV to areas of S100A9 expression, we hypothesize that these immune system processes become better localized to areas of tumor growth leading to increased efficacy. The targeted treatment acts broadly leading to rejection of tumor nodules throughout the intraperitoneal

space as evidenced by the survivors in the CPMV-H6/G3 groups. In comparison, the native CPMV, while it extends survival, did not produce any long-term survivors.

Biodistribution of S100A9-Targeted CPMV in CT26 Tumor-Bearing Mice.

CPMV is an immunomodulator and adjuvant and reverses immunosuppression within the TME through innate immune activation.[17] Therefore, CPMV primes a "hot" TME recruiting innate immune cells and natural killer cells to kill tumor cells and process tumor antigens leading to adaptive antitumor immunity.[20] By targeting the CPMV-H6/G3 to areas of S100A9 expression, we hypothesize that the S100A9-targeted CPMV is able to exert its function in a more tumor-localized manner compared to native CPMV, thereby leading to increased antitumor efficacy. To test this hypothesis, we performed biodistribution studies and confocal imaging of tumor sections.

For biodistribution analysis, dual fluorescent and S100A9-targeted CPMV particles were prepared as reported previously.[26] For these particles, an NHS-active ester of the Cy5 fluorophore is conjugated simultaneously with the $SMPEG_8$ linker to the exterior lysines of CPMV. Cy5-labeled CPMV particles were purified and characterized using the methods as mentioned above. UV–vis data revealed absorbance at 647 nm, indicating successful labeling with 54–69 Cy5 per CPMV (69 per CPMV and 58 and 54 per CPMV-H6/G3, respectively); the lower labeling of the latter is explained by the competing binding of Cy5 and $SMPEG_8$ (Figure S2a). Fluorescence imaging of the SDS-PAGE and agarose gels confirmed covalent attachment of the Cy5 comigrating with the CPs or intact particles; free dye was not apparent by either method (Figure S2b,c). The DLS data demonstrate monodisperse particles without any aggregation (Figure S2d), and this is further evidenced by the FPLC graphs (Figure S2e). For FPLC, we used a third detector at 647 nm, which again confirmed that the Cy5 dye coelutes with the intact CPMV particles.

The biodistribution of Cy5-CPMV vs Cy5-CPMV-H6/G3 was analyzed using ex vivo imaging of organs following intraperitoneal administration in intraperitoneal CT26-bearing mice (Figure 4a). In this experiment, 500,000 CT26 cells were injected IP followed by intraperitoneal injection of 200 μg of Cy5-CPMV, Cy5-CPMV-H6, Cy5-CPMV-G3, and PBS 1 week post tumor challenge. Tumor nodules dispersed throughout the intraperitoneal space were harvested the following day and combined for collective imaging on the IVIS (Figure S3). ROI measurements within Living Image 3.0 software were utilized to quantify the fluorescence signal within each of the organs. Quantitative analysis of tumors indicated 3.9-fold better accumulation of Cy5-CPMV-H6 vs Cy5-CPMV in the tumor tissue ($p < 0.01$), and a 2.9-fold improvement of Cy5-CPMV-G3 to Cy5-CPMV ($p < 0.05$) (Figure 4b,c). In a separate study, the biodistribution of the particles were analyzed in the reticuloendothelial organs as well as tumors. The dual fluorescent and peptide-conjugated particles were injected IP in tumor-bearing mice as before, and as a control, naïve mice were also injected. The tumors (only in tumor-inoculated mice), lungs, kidneys, spleen, and liver were harvested after 1 day and then imaged on the IVIS or through a plate reader (Figures S4–S6). IVIS imaging of tumors mirrored the results from the previous study (Figure S4). Because the excitation from IVIS imaging cannot penetrate throughout the entire tissue, the tumors were homogenized and the Cy5 fluorescence was measured on a plate reader

normalized to tumor weight. There were statistically insignificant trends pointing toward greater accumulation of Cy5-CPMV-H6 within the tumors followed by Cy5-CPMV-G3 and Cy5-CPMV, which identically mirrored the results from ex vivo imaging (Figures S4 and S5). Apart from differences in tumor accumulation, all formulations followed similar overall organ biodistribution in tumor-bearing and healthy mice with clearance mainly through the spleen and liver (Figure S6).

An additional assay measured the clearance of the CPMV particles from the intraperitoneal space with IVIS Cy5 imaging (Figure S7). There were no significant differences between CPMV particles in both tumor-bearing and naïve mice with clearance after 24 and 17 days, respectively, demonstrating that independent of the formulation, CPMV has good tumor retention properties. Furthermore, these data indicate that the improved therapeutic efficacy of the S100A9-targeted CPMV-H6/G3 most likely stems from improved tumor targeting due to the peptides but not due to enhanced retention within the intraperitoneal space.

Lastly, we performed colocalization studies of tumor sections using immunofluorescence staining and confocal microscopy. Tumor challenge was accomplished as outlined above, and tumors nodules were harvested after 24 h post single treatment with fluorescent CPMV. Tissues were sectioned and stained with α-S100A9 antibodies and Hoechst 33342. The sections were imaged on a confocal microscope, and the colocalization of the fluorescent CPMV and the stained S100A9 was visualized (Figures 4d and S8). Similar to the biodistribution assay, CPMV could be found within the tumor regardless of targeting, but S100A9-targeted CPMV-H6/G3 was more prominently found and more evenly distributed throughout the tumor nodules. Colocalization between CPMV-H6/G3 with S100A9 was evidenced by the merged images between the CPMV (green) and S100A9 (red). The colocalization as measured by the Mander's coefficient of the Cy5-CPMV:S100A9 was 0.168, while the coefficients of Cy5-CPMV-H6:S100A9 and Cy5-CPMV-G3:S100A9 were 0.516 and 0.497, respectively (Figure S9). Collectively these data indicate that the S100A9-targeting ligand confers increased tumor homing and increased tumor penetration through colocalization of S100A9.

S100A9 is expressed mainly by dendritic cells, neutrophils, and monocytes.[47] It is released into the extracellular tumor stroma by these cells, which then acts upon MDSCs directly increasing their immunosuppressive capabilities and further recruiting MDSC accumulation, thereby potentiating a positive feedback loop and additional S100A9 release.[36,48] We hypothesize that CPMV-H6/G3 improves targeting to S100A9-rich areas leading to reversal of the "cold" tumors into "hot" tumors and leading to potent antitumor efficacy. These data showcase that S100A9-targeted CPMV improves survival in mice with PM compared to native CPMV through the direct targeting of S100A9 and warrants further investigation into its use in the treatment of IP-disseminated tumors.

CONCLUSIONS

S100A9 becomes overexpressed within the TME of metastatic colon cancer increasing the immunosuppressive state of the tumors. CPMV particles can overcome the immunosuppressive TME when injected intratumorally, but direct intratumoral injections

are not possible with metastatic cancers. Targeting CPMV to S100A9 can overcome these barriers allowing for systemic CPMV injections. Indeed, treatment with S100A9-targeted CPMV-H6/G3 improves survival and decreases the weight gain and circumference increase caused by ascites formation in mice with IP-disseminated CT26 colon cancer. Ex vivo and immunofluorescence imaging of harvested tumors indicate that the S100A9 targeting improves CPMV accumulation within these tumors and colocalization of the CPMV-H6/G3 with S100A9. The ability of the CPMV particles to target areas of S100A9 through the conjugation of targeting peptides will allow for systemic administration of such particles and will open up the possibility of CPMV therapy in noninjectable tumors.

Supplementary Material

Refer to Web version on PubMed Central for supplementary material.

ACKNOWLEDGMENTS

This work was supported in part by the NIH (U01-CA218292, R01-CA224605, R01-CA253615, and R01 CA274640) and the Shaughnessy Family Fund for Nano-ImmunoEngineering (nanoIE) at UCSD. The Table of Contents graphic was created on Biorender.com.

REFERENCES

(1). Al-Shammaa HAH; Li Y; Yonemura Y Current Status and Future Strategies of Cytoreductive Surgery plus Intraperitoneal Hyperthermic Chemotherapy for Peritoneal Carcinomatosis. World J. Gastroenterol 2008, 14, 1159–1166. [PubMed: 18300340]

(2). Coccolini F; Gheza F; Lotti M; Virzì S; Iusco D; Ghermandi C; Melotti R; Baiocchi G; Giulini SM; Ansaloni L; Catena F Peritoneal Carcinomatosis. World J. Gastroenterol 2013, 19, 6979–6994. [PubMed: 24222942]

(3). Bando E; Yonemura Y; Takeshita Y; Taniguchi K; Yasui T; Yoshimitsu Y; Fushida S; Fujimura T; Nishimura G; Miwa K Intraoperative Lavage for Cytological Examination in 1,297 Patients with Gastric Carcinoma. Am. J. Surg 1999, 178, 256–262. [PubMed: 10527450]

(4). Gómez Portilla A; Cendoya I; López De Tejada I; Olabarría I; Martínez De Lecea C; Magrach L; Gil A; Echevarría J; Valdovinos M; Larrabide I Peritoneal Carcinomatosis of Colorectal Origin. Current Treatment. Review and Update. Rev. Esp. Enferm. Dig 2005, 97, 716–737. [PubMed: 16351464]

(5). Gadducci A; Cosio S; Conte PF; Genazzani AR Consolidation and Maintenance Treatments for Patients with Advanced Epithelial Ovarian Cancer in Complete Response after First-Line Chemotherapy: A Review of the Literature. Crit. Rev. Oncol. Hematol 2005, 55, 153–166. [PubMed: 15890524]

(6). Hugen N; van de Velde CJH; de Wilt JHW; Nagtegaal ID Metastatic Pattern in Colorectal Cancer Is Strongly Influenced by Histological Subtype. Ann. Oncol 2014, 25, 651–657. [PubMed: 24504447]

(7). Graversen M; Detlefsen S; Bjerregaard JK; Pfeiffer P; Mortensen MB Peritoneal Metastasis from Pancreatic Cancer Treated with Pressurized Intraperitoneal Aerosol Chemotherapy (PIPAC). Clin. Exp. Metastasis 2017, 34, 309–314. [PubMed: 28516306]

(8). del Castillo CF; Warshaw L Peritoneal Metastases in Pancreatic Carcinoma. Hepatogastroenterology 1993, 40, 430–432. [PubMed: 8270231]

(9). Tseng J; Bryan DS; Poli E; Sharma M; Polite BN; Turaga KK Under-Representation of Peritoneal Metastases in Published Clinical Trials of Metastatic Colorectal Cancer. Lancet Oncol. 2017, 18, 711–712. [PubMed: 28593843]

(10). Munker S; Gerken M; Fest P; Ott C; Schnoy E; Fichtner-Feigl S; Wiggermann P; Vogelhuber M; Herr W; Stroszczynski C; Schlitt HJ; Evert M; Reng M; Klinkhammer-Schalke M; Teufel A

Chemotherapy for Metastatic Colon Cancer: No Effect on Survival When the Dose Is Reduced Due to Side Effects. BMC Cancer 2018, 18, 455. [PubMed: 29685155]

(11). Hammond WA; Swaika A; Mody K Pharmacologic Resistance in Colorectal Cancer: A Review. Ther. Adv. Med. Oncol 2016, 8, 57–84. [PubMed: 26753006]

(12). Ushijima K Treatment for Recurrent Ovarian Cancer—At First Relapse. J. Oncol 2010, 2010, No. 497429.

(13). Kim S; Kim B; Song YS Ascites Modulates Cancer Cell Behavior, Contributing to Tumor Heterogeneity in Ovarian Cancer. Cancer Sci. 2016, 107, 1173–1178. [PubMed: 27297561]

(14). Sugarbaker PH Prevention and Treatment of Peritoneal Metastases: A Comprehensive Review. Indian J. Surg. Oncol 2019, 10, 3–23.

(15). Golshani G; Zhang Y Advances in Immunotherapy for Colorectal Cancer: A Review. Therap. Adv. Gastroenterol 2020, 13, No. 1756284820917527.

(16). Lin T; Chen Z; Usha R; Stauffacher CV; Dai JB; Schmidt T; Johnson JE The Refined Crystal Structure of Cowpea Mosaic Virus at 2. 8 A Resolution. Virology 1999, 265, 20–34. [PubMed: 10603314]

(17). Mao C; Beiss V; Fields J; Steinmetz NF; Fiering S Cowpea Mosaic Virus Stimulates Antitumor Immunity through Recognition by Multiple MYD88-Dependent Toll-like Receptors. Biomaterials 2021, 275, No. 120914.

(18). Lizotte PH; Wen AM; Sheen MR; Fields J; Rojanasopondist P; Steinmetz NF; Fiering S In Situ Vaccination with Cowpea Mosaic Virus Nanoparticles Suppresses Metastatic Cancer. Nat. Nanotechnol 2016, 11, 295–303. [PubMed: 26689376]

(19). Murray AA; Wang C; Fiering S; Steinmetz NF In Situ Vaccination with Cowpea vs Tobacco Mosaic Virus against Melanoma. Mol. Pharmaceutics 2018, 15, 3700–3716.

(20). Wang C; Fiering SN; Steinmetz NF Cowpea Mosaic Virus Promotes Anti-Tumor Activity and Immune Memory in a Mouse Ovarian Tumor Model. Adv. Ther 2019, 2, No. 1900003.

(21). Shukla S; Wang C; Beiss V; Steinmetz NF Antibody Response against Cowpea Mosaic Viral Nanoparticles Improves In Situ Vaccine Efficacy in Ovarian Cancer. ACS Nano 2020, 14, 2994–3003. [PubMed: 32133838]

(22). Shukla S; Wang C; Beiss V; Cai H; Washington T; Murray AA; Gong X; Zhao Z; Masarapu H; Zlotnick A; Fiering S; Steinmetz NF The Unique Potency of Cowpea Mosaic Virus (CPMV) in Situ Cancer Vaccine. Biomater. Sci 2020, 8, 5489–5503. [PubMed: 32914796]

(23). Kerstetter-Fogle A; Shukla S; Wang C; Beiss V; Harris PLR; Sloan AE; Steinmetz NF Plant Virus-Like Particle In Situ Vaccine for Intracranial Glioma Immunotherapy. Cancers 2019, 11, 515. [PubMed: 30974896]

(24). Hoopes PJ; Wagner RJ; Duval K; Kang K; Gladstone DJ; Moodie KL; Crary-Burney M; Ariaspulido H; Veliz FA; Steinmetz NF; Fiering SN Treatment of Canine Oral Melanoma with Nanotechnology-Based Immunotherapy and Radiation. Mol. Pharmaceutics 2018, 15, 3717–3722.

(25). Alonso-Miguel D; Valdivia G; Guerrera D; Perez-Alenza MD; Pantelyushin S; Alonso-Diez A; Beiss V; Fiering S; Steinmetz NF; Suarez-Redondo M; Berg J; Peña L; Arias-Pulido H Neoadjuvant in Situ Vaccination with Cowpea Mosaic Virus as a Novel Therapy against Canine Inflammatory Mammary Cancer. J. Immunother. Cancer 2022, 10, No. e004044.

(26). Chung YH; Park J; Cai H; Steinmetz NF S100A9-Targeted Cowpea Mosaic Virus as a Prophylactic and Therapeutic Immunotherapy against Metastatic Breast Cancer and Melanoma. Adv. Sci 2021, 8, No. 2101796.

(27). Qin H; Lerman B; Sakamaki I; Wei G; Cha SC; Rao SS; Qian J; Hailemichael Y; Nurieva R; Dwyer KC; Roth J; Yi Q; Overwijk WW; Kwak LW Generation of a New Therapeutic Peptide That Depletes Myeloid-Derived Suppressor Cells in Tumor Bearing Mice. Nat. Med 2014, 20, 676–681. [PubMed: 24859530]

(28). Park J; Wen AM; Gao H; Shin MD; Simon DI; Wang Y; Steinmetz NF Designing S100A9-Targeted Plant Virus Nanoparticles to Target Deep Vein Thrombosis. Biomacromolecules 2021, 22, 2582–2594. [PubMed: 34060817]

(29). Markowitz J; Carson WE Review of S100A9 Biology and Its Role in Cancer. Biochim. Biophys. Acta 2013, 1835, 100–109. [PubMed: 23123827]

(30). Wang S; Song R; Wang Z; Jing Z; Wang S; Ma J S100A8/A9 in Inflammation. Front. Immunol 2018, 9, 1298. [PubMed: 29942307]

(31). Edgeworth J; Gorman M; Bennett R; Freemont P; Hogg N Identification of P8,14 as a Highly Abundant Heterodimeric Calcium Binding Protein Complex of Myeloid Cells. J. Biol. Chem 1991, 266, 7706–7713. [PubMed: 2019594]

(32). Hunter MJ; Chazin WJ High Level Expression and Dimer Characterization of the S100 EF-Hand Proteins, Migration Inhibitory Factor-Related Proteins 8 and 14. J. Biol. Chem 1998, 273, 12427–12435. [PubMed: 9575199]

(33). Gebhardt C; Németh J; Angel P; Hess J S100A8 and S100A9 in Inflammation and Cancer. Biochem. Pharmacol 2006, 72, 1622–1631. [PubMed: 16846592]

(34). Németh J; Stein I; Haag D; Riehl A; Longerich T; Horwitz E; Breuhahn K; Gebhardt C; Schirmacher P; Hahn M; Ben-Neriah Y; Pikarsky E; Angel P; Hess J S100A8 and S100A9 Are Novel Nuclear Factor Kappa B Target Genes during Malignant Progression of Murine and Human Liver Carcinogenesis. Hepatology 2009, 50, 1251–1262. [PubMed: 19670424]

(35). Ghoneum A; Afify H; Salih Z; Kelly M; Said N Role of Tumor Microenvironment in the Pathobiology of Ovarian Cancer: Insights and Therapeutic Opportunities. Cancer Med. 2018, 7, 5047–5056. [PubMed: 30133163]

(36). Srikrishna G S100A8 and S100A9: New Insights into Their Roles in Malignancy. J. Innate Immun 2011, 4, 31–40. [PubMed: 21912088]

(37). Fang W-Y; Chen Y-W; Hsiao J-R; Liu C-S; Kuo Y-Z; Wang Y-C; Chang K-C; Tsai S-T; Chang M-Z; Lin S-H; Wu L-W Elevated S100A9 Expression in Tumor Stroma Functions as an Early Recurrence Marker for Early-Stage Oral Cancer Patients through Increased Tumor Cell Invasion, Angiogenesis, Macrophage Recruitment and Interleukin-6 Production. Oncotarget 2015, 6, 28401–28424. [PubMed: 26315114]

(38). Lv Z; Li W; Wei X S100A9 Promotes Prostate Cancer Cell Invasion by Activating TLR4/NF-KB/Integrin B1/FAK Signaling. Onco Targets Ther. 2020, 13, 6443–6452. [PubMed: 32884282]

(39). Hwang S-H; Ahn J-H; Lee M Upregulation of S100A9 Contributes to the Acquired Resistance to BRAF Inhibitors. Genes Genomics 2019, 41, 1273–1280. [PubMed: 31388978]

(40). Meng J; Gu F; Fang H; Qu B Elevated Serum S100A9 Indicated Poor Prognosis in Hepatocellular Carcinoma after Curative Resection. J. Cancer 2019, 10, 408–415. [PubMed: 30719134]

(41). Liao J; Li J-Z; Xu J; Xu Y; Wen W-P; Zheng L; Li L High S100A9+ Cell Density Predicts a Poor Prognosis in Hepatocellular Carcinoma Patients after Curative Resection. Aging 2021, 13, 16367–16380. [PubMed: 34157683]

(42). Ichikawa M; Williams R; Wang L; Vogl T; Srikrishna G S100A8/A9 Activate Key Genes and Pathways in Colon Tumor Progression. Mol. Cancer Res 2011, 9, 133–148. [PubMed: 21228116]

(43). Duan L; Wu R; Ye L; Wang H; Yang X; Zhang Y; Chen X; Zuo G; Zhang Y; Weng Y; Luo J; Tang M; Shi Q; He T; Zhou L S100A8 and S100A9 Are Associated with Colorectal Carcinoma Progression and Contribute to Colorectal Carcinoma Cell Survival and Migration via Wnt/β-Catenin Pathway. PLoS One 2013, 8, No. e62092.

(44). Turovskaya O; Foell D; Sinha P; Vogl T; Newlin R; Nayak J; Nguyen M; Olsson A; Nawroth PP; Bierhaus A; Varki N; Kronenberg M; Freeze HH; Srikrishna G RAGE, Carboxylated Glycans and S100A8/A9 Play Essential Roles in Colitis-Associated Carcinogenesis. Carcinogenesis 2008, 29, 2035–2043. [PubMed: 18689872]

(45). Sinha P; Okoro C; Foell D; Freeze HH; Ostrand-Rosenberg S; Srikrishna G Proinflammatory S100 Proteins Regulate the Accumulation of Myeloid-Derived Suppressor Cells. J. Immunol 2008, 181, 4666–4675. [PubMed: 18802069]

(46). Ba M; Chen C; Long H; Gong Y; Wu Y; Lin K; Tu Y; Zhang B; Wu W Cytoreductive Surgery and HIPEC for Malignant Ascites from Colorectal Cancer - a Randomized Study. Medicine 2020, 99, No. e21546.

(47). Averill MM; Barnhart S; Becker L; Li X; Heinecke JW; LeBoeuf RC; Hamerman JA; Sorg C; Kerkhoff C; Bornfeldt KE S100A9 Differentially Modifies Phenotypic States of Neutrophils, Macrophages, and Dendritic Cells. Circulation 2011, 123, 1216–1226. [PubMed: 21382888]

(48). Huang M; Wu R; Chen L; Peng Q; Li S; Zhang Y; Zhou L; Duan L S100A9 Regulates MDSCs-Mediated Immune Suppression via the RAGE and TLR4 Signaling Pathways in Colorectal Carcinoma. Front. Immunol 2019, 10, 2243. [PubMed: 31620141]

(49). Wen AM; Lee KL; Yildiz I; Bruckman MA; Shukla S; Steinmetz NF Viral Nanoparticles for In Vivo Tumor Imaging. J. Visualized Exp 2012, 69, No. e4532.

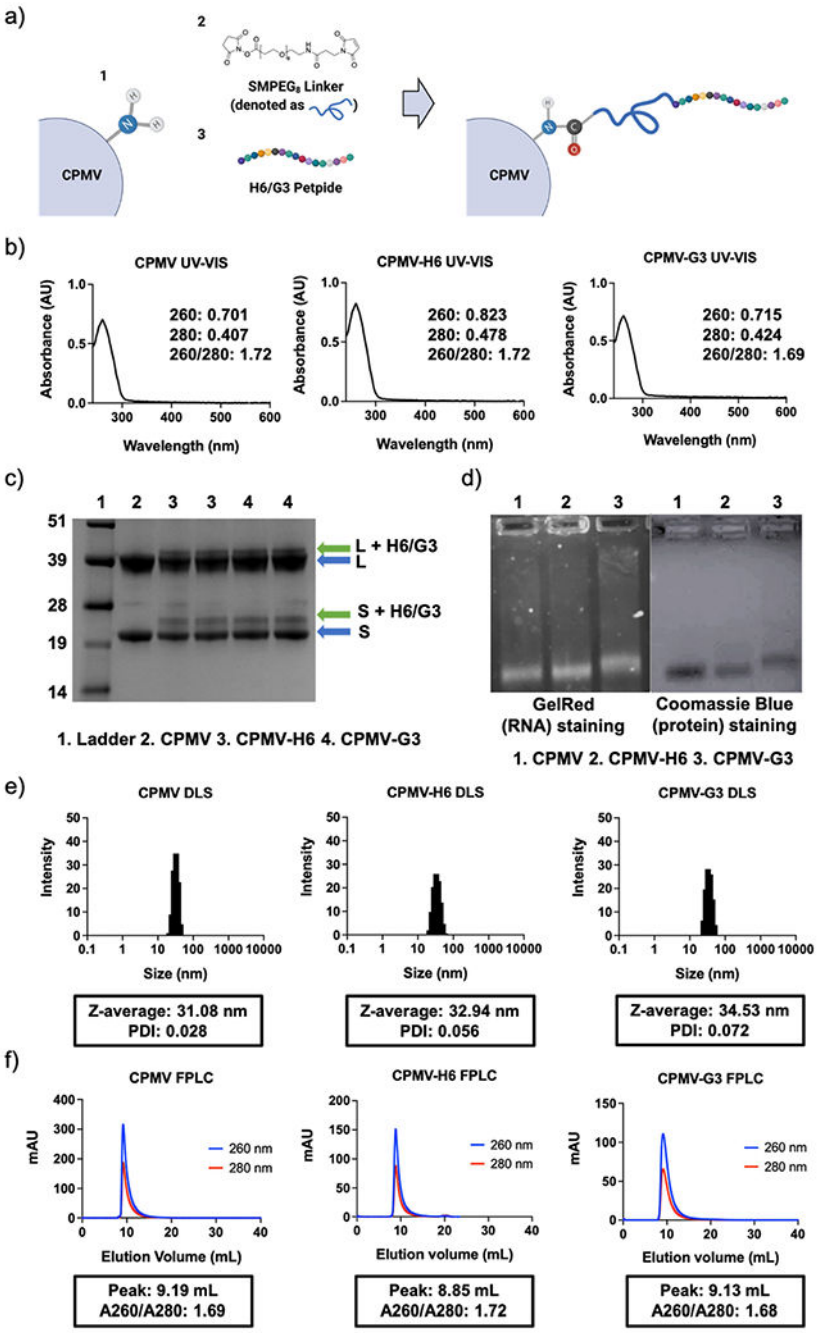

Figure 1.

Characterization of S100A9-targeted CPMV particles. (a) Schematic showcasing the protocol for conjugation of the H6 and G3 peptides onto CPMV. All images were created on Biorender.com. (b) UV–vis spectra of the S100A9-targeted particles. The inset is displaying the absorbance at 260 and 280 nm as well as the absorbance ratio between 260 and 280 nm. A ratio of 1.8 indicates pure, intact particles. (c) SDS-PAGE of the S100A9-targeted particles. The additional, higher molecular weight bands above the small and large CP of CPMV indicates conjugation of the H6 or G3 peptide. (d) Agarose gel electrophoresis of

the S100A9-targeted particles. The RNA is stained with GelRed, and the protein is stained with Coomassie Blue. Identical electrophoretic mobility down the gels between the RNA and protein indicate intact particles. (e) DLS spectra of S100A9-targeted particles. The box below the DLS indicates the average size of the particles as well as the PDI. (f) FPLC graphs of the S100A9-targeted particles. The absorbance was measured at 260 and 280 nm, and the box below the graphs is displaying the peak elution volume, as well as the absorbance ratio between 260 and 280 nm at that peak.

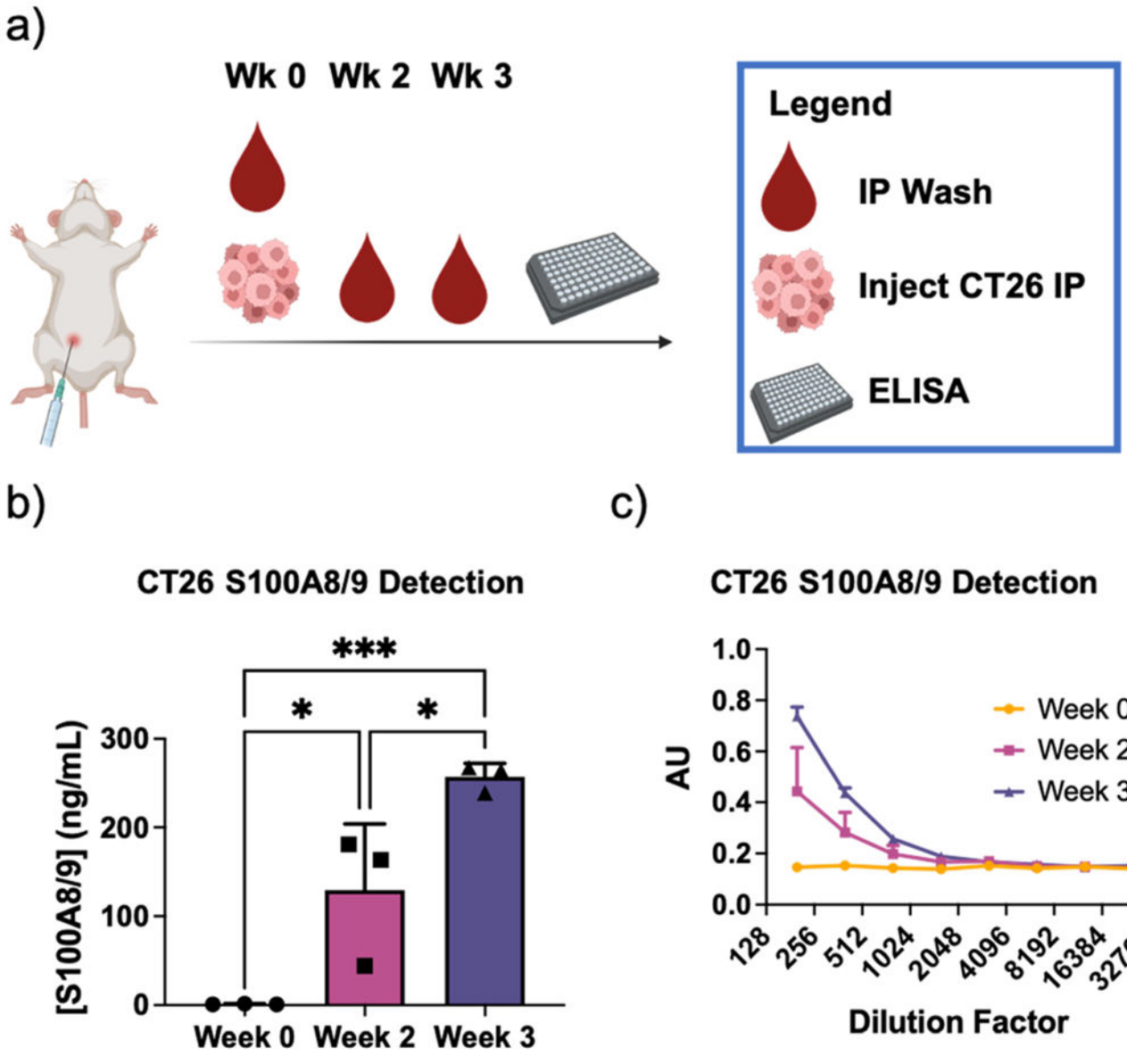

Figure 2.

ELISA detection of S100A8/9 within the intraperitoneal fluid. (a) Schedule of the CT26 tumor injection as well as the intraperitoneal fluid collection. All images were created on Biorender.com. (b) ELISA analysis of S100A8/9 concentrations within the intraperitoneal fluid at weeks 0, 2, and 3. (c) Full ELISA spectra for (b) at all timepoints. All analyses were done by one- or two-way ANOVA. * $p < 0.05$, *** $p < 0.001$.

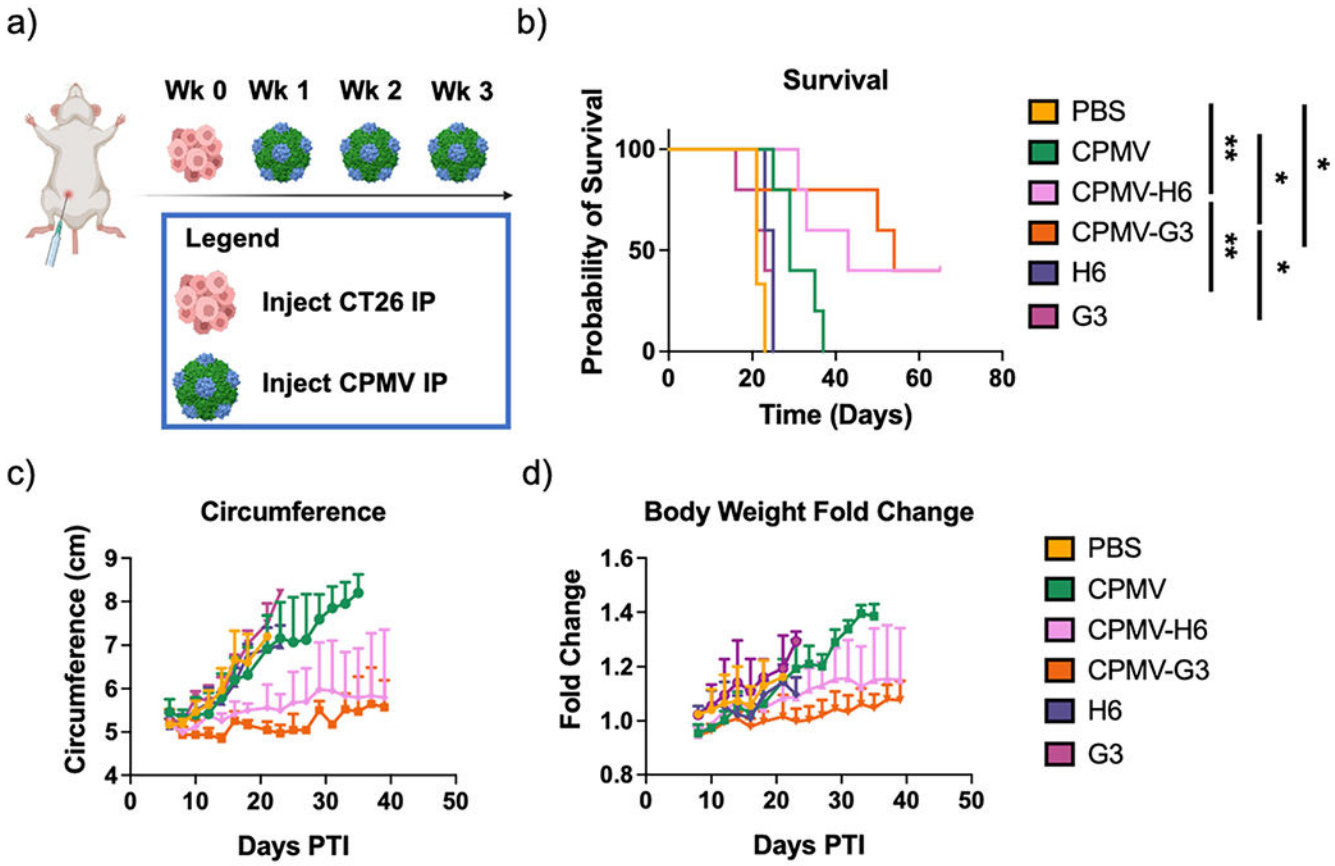

Figure 3.

CT26 treatment efficacy with S100A9-targeted CPMV. (a) Injection schedule of the CT26 and CPMV particles. All images were created on Biorender.com. (b) Survival curves of the mice following treatment with S100A9-targeted CPMV. Analyses were done using the log-rank (Mantel-Cox) test. (c) Change in the maximum abdominal circumference compared to the circumference at day 0 before tumor inoculation. The circumference was measured every 2 days starting on day 8 post tumor inoculation. (d) Body weight change compared to day 0 before tumor inoculation. The body weight was measured every 2 days starting on day 8 post tumor inoculation. * $p < 0.05$, ** $p < 0.01$.

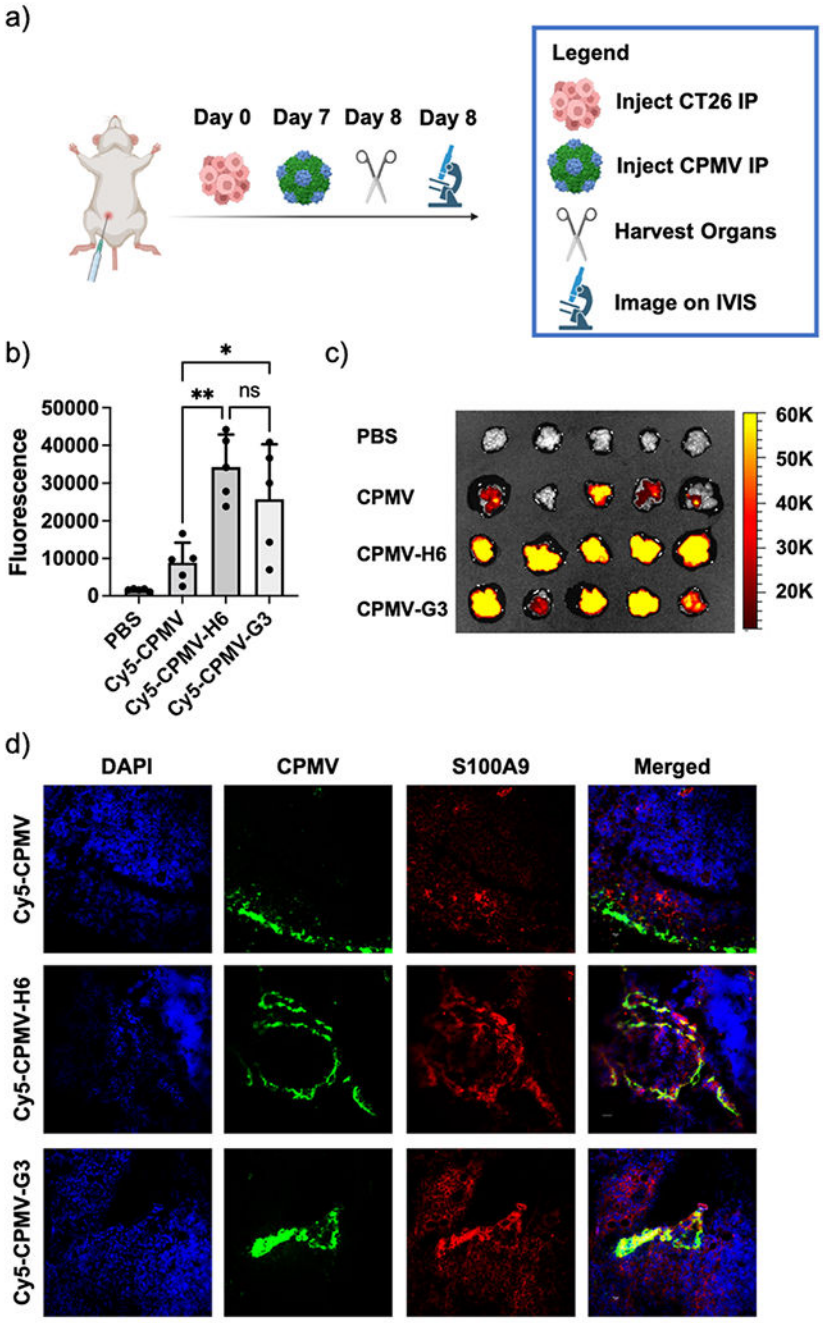

Figure 4.

Biodistribution and S100A9 colocalization following injection with S100A9-targeted CPMV. (a) Injection schedule of the CT26 tumors and CPMV followed by organ harvesting and imaging. All images were created on Biorender.com. (b) Quantitative analysis of the ROI fluorescence from ex vivo imaging or harvested tumors following CPMV injection. The particles were conjugated with Cy5. (c) Qualitative images of the harvested tumors following CPMV injection. (d) Immunofluorescence staining of tumor sections. The sections were stained with DAPI and α-S100A9 antibodies. The CPMV was visualized through

conjugated Cy5 fluorophores. The statistical analysis in (b) was analyzed using one-way ANOVA. * $p < 0.05$, ** $p < 0.01$, ns = not significant.